Research Article

Received: 13 December 2019 Revised: 17 March 2020 Accepted article published: 3 April 2020 Published online in Wiley Online Library:

(wileyonlinelibrary.com) DOI 10.1002/pi.6012

Development of waste tire-derived graphene reinforced polypropylene nanocomposites with controlled polymer grade, crystallization and mechanical characteristics via melt-mixing

Jamal Seyyed Monfared Zanjani,[a] Leila Haghighi Poudeh,[b] Burcu Girginer Ozunlu,[c,d] Yavuz Emre Yagci,[c] Yusuf Menceloglu[b,e] and Burcu Saner Okan[b*]

Abstract

In the present work, single layer graphene nanoplatelets (GNPs) derived from waste tires by recycling and upcycling approaches were integrated in homopolymer (Homo-) and copolymer (Copo-) polypropylene (PP) matrices by fast and efficient mixing in the melt phase. The effect of GNP content on crystallization and mechanical behaviors was investigated in detail at different loading levels. Regarding isothermal and non-isothermal crystallization experiments, GNPs significantly accelerated the nucleation and growth of crystallites, and the crystallization degree in Homo-PP nanocomposites was slightly higher than that of Copo-PP based nanocomposites. Also, there was significant improvement in mechanical and thermal properties of GNP reinforced polymers compared to neat polymers. As the GNP concentration increased from 1 to 5 wt%, there was a gradual increase in flexural modulus and strength values. In tensile tests, an increase in GNP content in both polymer grades led to a slight increase in yield strength coming from the proper distribution of nano-reinforcement by creating stress concentration sites. After the yield point, Homo-PP based nanocomposites showed higher strain hardening than GNP reinforced Copo-PP owing to a high crystallization degree and linear chains of Homo-PP. This work showed that functionalized graphene can act as both nucleating and reinforcing agent in the compounding process and its exfoliation through polymer chains is much better in homopolymers at a faster and high shear rate.

Supporting information may be found in the online version of this article.

Keywords: graphene; waste materials; polymer-matrix composites; mechanical properties; thermal properties

INTRODUCTION

Polypropylene (PP), a semicrystalline thermoplastic polymer, has drawn great attention as a matrix for polymeric composites due to its ease of fabrication, low cost and recyclability.[1] However, in industrial applications, PP has some limitations since it suffers from high molding shrinkage, low impact factor and poor toughness.[2] Therefore, in the last few years, great efforts have been made to balance rigidity–impact strength by controlling the crystallinity and thus enhancing the performance of PP based polymeric composites in several fields such as the automotive, electronics and packaging industries.[3] These techniques are divided into two main categories, which are the insertion of co-monomers and the addition of nucleating agents in the polymer matrix.

In the first approach, PP is modified by introducing randomly distributed co-monomer units such as ethylene to the crystal lattice of the polymer which reduces the crystallinity and enables the modification of macroscopic properties of the PP polymer.[4] For instance,

* *Correspondence to: B.S. Okan, Sabanci University Integrated Manufacturing Technologies Research and Application Center and Composite Technologies Center of Excellence, Teknopark Istanbul, 34906, Pendik, Istanbul, Turkey. E-mail: burcu.saner@sabanciuniv.edu*

a *Faculty of Engineering Technology, University of Twente, Enschede, The Netherlands*

b *Sabanci University Integrated Manufacturing Technologies Research and Application Center & Composite Technologies Center of Excellence, Manufacturing Technologies, Istanbul, Turkey*

c *Farplas Otomotiv A.S., Taysad Organize Sanayi Bölgesi (TOSB), Kocaeli, Turkey*

d *Istanbul Technical University, Faculty of Chemical and Metallurgical Engineering, Metallurgical and Materials Engineering, Istanbul, Turkey*

e *Faculty of Engineering and Natural Sciences, Materials Science and Nano Engineering, Sabanci University, Istanbul, Turkey*

Benavente *et al.*[5] showed that PP copolymer with ethylene had lower stiffness and Young's modulus compared to neat PP due to the decrease in crystallinity of the copolymer. In the second approach, the integration of carbon based materials like graphene[6,7] and carbon nanotubes[8] into the PP matrix is known to induce a crystalline structure by acting as a nucleating agent at the surface of the polymer and thus increases the crystallization temperature, crystallization rate and degree of crystallinity.[9] In particular, graphene improves the mechanical, thermal and electrical properties of PP composites due its two-dimensional structure and surface chemistry.[10]

Among various composite fabrication techniques, solution processing,[10] *in situ* polymerization[6] and melt compounding[11] have been widely used to fabricate PP/graphene composites. For industrial processes, melt compounding is a widely preferred technique since it is economically feasible and does not need any solvents.[12] In this technique, graphene is added to the molten polymer at temperature of 30–60 °C above the melting point of PP.[14] Nevertheless, one of the major challenges in the production of PP/graphene composites is to get a homogeneous dispersion of graphene in the polymeric matrix since the performance of graphene based polymeric composites improves only by providing homogeneous dispersion and strong interfacial adhesion between graphene and the polymer matrix.[13] Up to now, numerous studies have reported on the enhancement of the mechanical and thermal properties of PP polymer by the incorporation of graphene into the polymer matrix through the melt compounding process.[7,14] In one of the studies, graphene oxide synthesized by the modified Hummers method[15] was coated on PP latex, which is a water based emulsion of maleic anhydride grafted isotactic PP, and was then compounded with PP polymer in the melt phase.[13] This work provided an increase of 75% in the yield strength and 74% in Young's modulus, and the glass transition temperature and initial degradation temperature of PP were enhanced by 2.5 and 26 °C at only 1 wt% of graphene loading.[13] In another study, graphene nanoplatelets (GNPs) were directly compounded with homopolymer PP (Homo-PP) by an extrusion process; an improvement of 150% was achieved in the case of Young's modulus as well as a reduction in the elongation at failure from 250% to 10%.[16] Therefore, the crystallinity of PP polymer has a significant influence on the mechanical and thermal properties of PP based composites.

It is important to note that the changes in the structure of the polymer and the presence of a second phase such as graphene can affect the mechanical and thermal properties of graphene based composites. Although several authors have studied the effect of GNPs on the characteristics of various polymeric composites,[17–21] to the best of our knowledge, there is no related work that investigates how the polymer grades and graphene content affect the mechanical and thermal characteristics of graphene based PP nanocomposites simultaneously and systematically. In this work, GNP reinforced Homo-PP and copolymer PP (Copo-PP) nanocomposites were fabricated by the melt compounding technique and the effects of different amounts of GNPs as well as the type of polymer grade on the mechanical, thermal and structural properties of the composite were examined in detail.

MATERIALS AND METHODS

Materials

GNPs produced from waste tires by recycling and upcycling processes were purchased from Nanografen Co., Istanbul, Turkey. PP homopolymer (HE125 MO) with good flow properties and high stiffness was received from Borealis, Vienna, Austria. PP copolymer (Kopelen JM-365), a high impact block copolymer, was provided from Seoul, South Korea, and contained high ethylene-polypropylene rubber content. Both polymer grades are suitable for injection molding. The changes in the storage modulus and viscosity of Homo-PP and Copo-PP as a function of time and temperature are given in Fig. S1.

Preparation of GNP reinforced Homo- and Copo-PP nanocomposites

GNP reinforced Homo-PP and Copo-PP nanocomposites were prepared by a custom-made Gelimat thermokinetic mixing/compounding machine at a shear rate of 5500 rpm at 215 °C for 45 s. The compounds obtained were injected by an Explore injection machine into tensile and bending test specimens in conformity with ISO 527-2 and ASTM-D790, respectively.

Characterization

Differential Scanning Calorimetry (DSC) measurements of polymers and nanocomposites were carried out under a nitrogen atmosphere from 20 to 200 °C using a Mettler Toledo DSC 3+ 700. About 7 mg of the dried sample was heated and held at 200 °C for 5 min to eliminate thermal history. To determine the crystallization and melting properties, the second heating and first cooling cycles were performed at a rate of 10 °C min^{-1}. The associated thermal parameters of crystallization (T_c) and melting (T_m) temperatures, crystallization enthalpy (ΔH_c) and the heat of melting (ΔH_m) were extracted using STARe software provided by Mettler Toledo. Furthermore, various cooling rates (2, 5, 10, 20 and 40 °C min^{-1}) were applied to analyze the non-isothermal crystallization. The morphology of the nanocomposites was examined with a Leo Supra 35VP field emission scanning electron microscope and a JEOL 2100 Lab6 high resolution transmission electron microscope. The specimens were fractured in liquid nitrogen and coated with a thin gold layer before SEM observation. X-ray diffraction (XRD) analysis was carried out using a Bruker D2 Phaser Desktop diffractometer with a Cu Kα radiation source. X-ray photoelectron spectroscopy (XPS) was used for elemental analysis of the graphene samples. The mechanical tests were conducted using an Instron 5982 Static Universal Test Machine with a 5 kN load cell for tensile and bending tests. The samples were analyzed by TGA using a Toledo TGA/DSC 3+ 1600 thermal analyzer under a nitrogen atmosphere from 25 to 600 °C at a rate of 10 °C min^{-1}. Rheological characterization of the specimens was conducted using an MCR 702 TwinDrive Anton Paar rheometer.

RESULTS AND DISCUSSION

GNP characteristic properties

The surface functional groups, morphology and structural properties of graphene play an important role in producing composites with desired properties.[22,23] In the present study, graphene nanoplatelets produced from the recycling process of waste tires was used as a reinforcing agent. GNPs derived from pyrolyzed waste tires have 87 wt% carbon and 9.1 wt% oxygen functional groups on the surface, measured by X-ray photoelectron spectroscopy (Fig. S2(a)). This graphene has characteristic graphene peaks of D and G bands at around 1358 and 1580 cm^{-1}, respectively, as seen in Fig. S2(b). Also, the SEM image in Fig. S2(c) indicates platelet formation after the recycling process. The TEM image of GNPs in Fig. S2(d) shows platelet structures having an average length of 50 nm. The Brunauer–Emmett–Teller surface area was measured as 85 m^2 g^{-1}.

Crystallization and melting properties of GNP based PP nanocomposites

The effect of GNP on non-isothermal crystallization behaviors of nanocomposites

The physical and mechanical properties of semicrystalline thermoplastics of Homo- and Copo-PP are in close correlation with their microstructure and crystallinity state. Herein, the melting and crystallization behavior of both Homo- and Copo-PP and their nanocomposites with GNPs were studied under non-isothermal conditions as a function of GNP loading. Figure 1 reveals the crystallization and melting curves of Homo- and Copo-PP neat specimens and their nanocomposites after the elimination of thermal history of the specimens at 200 °C for 5 min. The parameters extracted from these experiments are summarized in Table 1. The crystallization temperature measured from the first cooling cycle of DSC measurements was found to increase on the addition of GNPs for both types of PP. In Homo-PP, the crystallization onset temperature sharply increased from 122 °C for neat Homo-PP to 134 °C on the implementation of only 1 wt% GNP, and further increased on increasing the GNP content to reach 136 °C at both 3 wt% and 5 wt% GNP loading, as shown in Fig. 1(a). A similar trend of increased crystallization onset temperature was also observed for Copo-PP in which neat Copo-PP showed a crystallization onset temperature of 120 °C while the presence of 1 wt% GNP shifted the crystallization initiation temperature to 127 °C and further increase in GNP content slightly increased the temperature to 128 and 129 °C in specimens with 3 wt% and 5 wt% GNP amounts, respectively, as exhibited in Fig. 1(b). The increases observed in the crystallization onset temperatures indicate that the GNPs act as nucleation agent and promote the crystallization of both PP grades during the cooling cycle.[12] A similar trend of increase in the crystallization onset temperature was also reported in the literature.[24–27] In addition, a higher increase in crystallization onset temperature for nanocomposites based on Homo-PP compared to Copo-PP means that the Homo-PP structure is more prone to crystallization than Copo-PP. In addition, considering the crystallization enthalpy, ΔH_c showed a higher crystallinity level of Homo-PP in comparison with Copo-PP as anticipated from their molecular structures. Additionally, the integration of 1 wt% GNP in both grades of PP increased ΔH_c sharply while a further increase showed a reduction of ΔH_c, as presented in Table 1. This may stem from the change in size of the crystals on increasing the GNP concentration.[28] The higher GNP content in both polymer grades leads to a higher number of nucleation sites but a smaller crystal size in the structure can consequently lower the overall crystallinity compared to 1 wt% reinforced specimens.[28] The results from the second heating curves in Fig. 1 (c) and 1(d) show that the values of the initiation of melting for both polymer grades increase on adding GNPs but these increases are on much smaller scales compared to the crystallization temperature in the cooling cycle. It is worth noting that the differences in melting points between neat PP specimens and GNP reinforced PP nanocomposites stem from the formation of different crystal structures in these materials. In neat specimens, crystallization started at lower temperatures and created more β-form crystals having a lower melting point, Young's modulus and yield stress compared to the α-form created at higher temperatures.[29,30] The α-form is a thermodynamically stable phase and has good mechanical strength, resulting from the cross-hatched lamellar morphology and compact stacking of molecular chains, while the β-form is a thermodynamically metastable phase, which can be obtained under special conditions such as in the presence of certain heterogeneous nucleating agents like GNPs.[31] The results from the melting curves revealed the possibility of the presence of β-crystalline structure in the neat specimens, which was eliminated in nanocomposite structures;

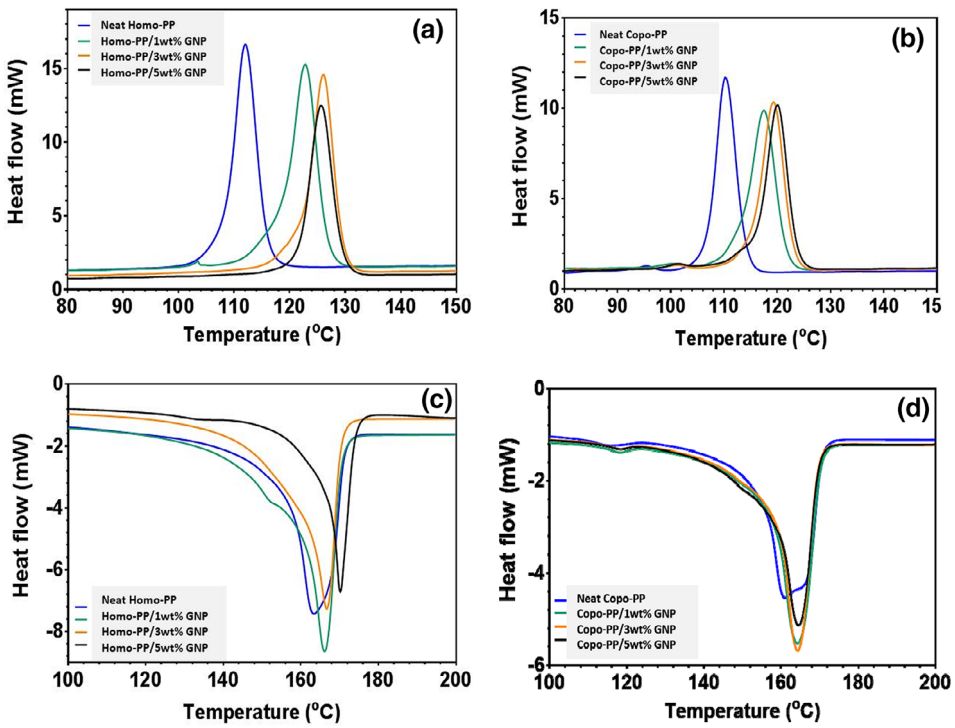

Figure 1. DSC thermograms of the crystallization in the first cooling cycle of (a) Homo-PP and (b) Copo-PP and their nanocomposites with GNPs, and melting curves in the second heating cycle of (c) Homo-PP and (d) Copo-PP and their nanocomposites with GNPs.

Table 1. Summary of the thermal parameters of neat and GNP based specimens extracted from DSC measurements

Specimen type	Melting onset temperature (°C)	Melting peak temperature (°C)	Melting integral, ΔH_m (J g^{-1})	Crystallization onset temperature (°C)	Crystallization peak temperature (°C)	Crystallization integral ΔH_c (J g^{-1})
Neat Homo-PP	119	163	−95.60	122	113	95.60
Homo-PP/1 wt% GNP	121	166	−106.48	134	124	105.07
Homo-PP/3 wt% GNP	121	166	−99.24	136	127	99.07
Homo-PP/5 wt% GNP	124	170	−101.48	136	126	100.80
Neat Copo-PP	125	161	−63.14	120	111	63.78
Copo-PP/1 wt% GNP	123	164	−68.23	127	118	69.96
Copo-PP/3 wt% GNP	123	164	−70.24	128	120	71.2
Copo-PP/5 wt% GNP	123	164	−64.48	129	121	63.86

further investigation was done by XRD described in the next section.

In order to elaborate on the crystallization behavior of neat PP and its nanocomposites, Homo-PP, Copo-PP and 3 wt% GNP reinforced Homo- and Copo-PP specimens were examined by DSC at different temperature change rates ranging from −2 to −40 °C min^{-1} as presented in Fig. 2. Regarding the improvement percentages in melting and crystallization temperatures, the ideal amount of GNP was decided as 3 wt% and a comparison of non-isothermal crystallization behavior between neat and 3 wt% GNP based nanocomposites was done. It can be seen that, as cooling rates increased, crystallization peaks became wider and shifted to lower temperatures in all specimens, indicating the time-dependent nucleation and crystal growth of PP polymer.[28,32] Figure 3 presents the values for the crystallization initiation temperature (T_0) and the difference between the crystallization initiation temperature and peak temperature ($T_0 - T_p$) of selected specimens. As is obvious in Figs 3(a) and 3(c), the incorporation of GNPs into both Homo-PP and Copo-PP matrices shifted the T_0 to higher temperature at all cooling rates due to an increase in nucleation sites. On the other hand, nanocomposite specimens of both polymer grades showed a sharper crystallization peak compared to neat specimens, which was verified in the value of $T_0 - T_p$ in Figs 3(b) and 3(d) as an indication of crystallization rate and showing a higher crystallization rate for nanocomposite specimens. The deviation at low cooling (below 10 °C min^{-1}) stems from the difference in crystal forms at low and high temperatures where due to initiation of crystallization at higher temperature, it is dominated by the α-form.

Crystal structure analysis by X-ray diffraction (XRD)

In order to further understand the effect of GNPs on the crystal structure of both Homo-PP and Copo-PP, XRD patterns obtained for neat specimens and specimens reinforced by 3 wt% GNP are presented in Fig. 4. The Homo-PP and its nanocomposites have the characteristic reflections of (110) at $2\theta = 14.4°$, (040) at

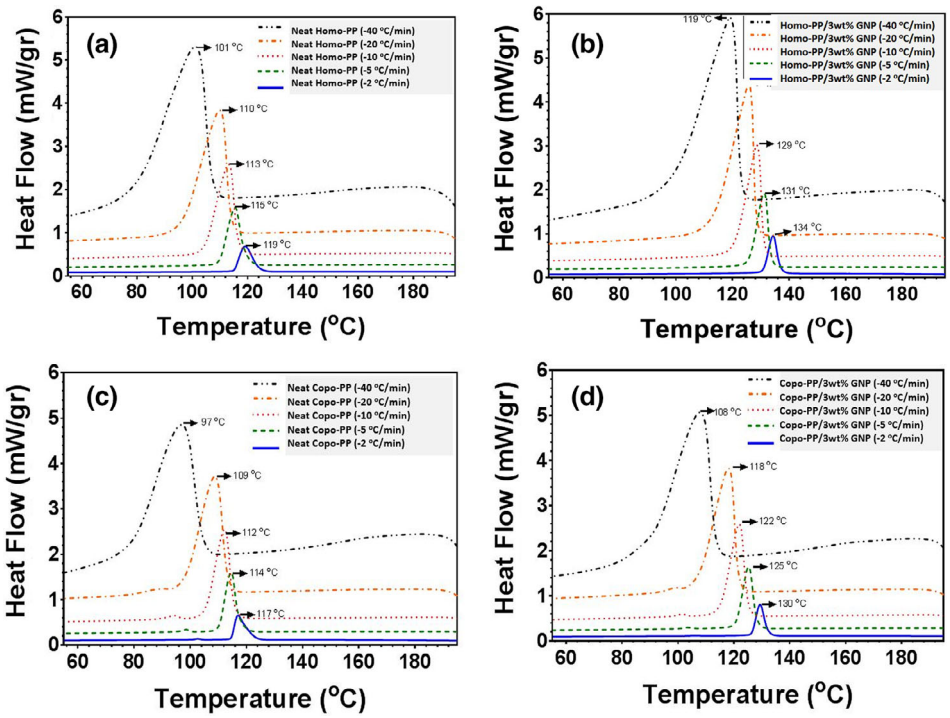

Figure 2. DSC thermograms of non-isothermal crystallization for (a) neat Homo-PP, (b) Homo-PP/3 wt% GNP, (c) neat Copo-PP and (d) Copo-PP/3 wt% GNP at different cooling rates.

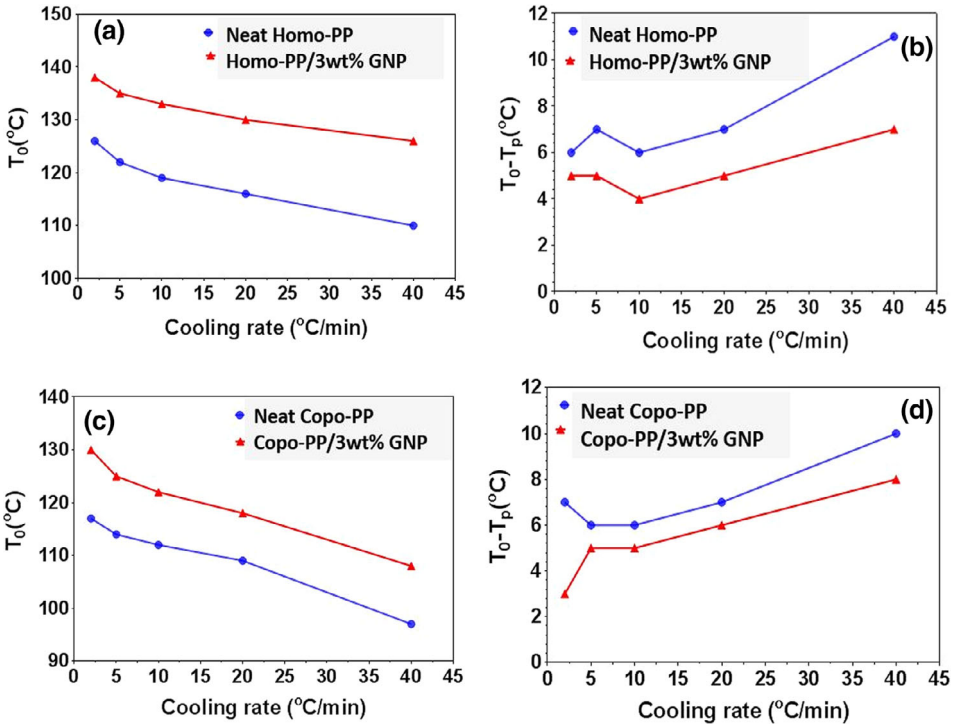

Figure 3. The values of T_0 and $T_0 - T_p$ for (a), (b) Homo-PP and (c), (d) Copo-PP and their 3 wt% GNP reinforced nanocomposites as a function of cooling rate.

$2\theta = 17.3°$, (130) at $2\theta = 18.9°$ and (131) at $2\theta = 21.8°$ representing the α crystal structure.[28] The attention grabbing phenomenon is the shoulder peak around $2\theta = 16.4°$ for neat Homo-PP which corresponds to the coexistence of a small amount of β phase in the structure which disappears after the integration of GNPs with a tendency to induce α phase crystals.[29] Compared to Homo-PP, the presence of another monomer in the structure of Copo-PP (ethylene) introduces more disorder in the lattice structure of the copolymer causing wider diffraction peaks.[33] On the other hand, in the Copo-PP the β crystalline peak at $2\theta = 16.4°$ is clearly seen for neat specimens and completely disappears for specimens with GNPs. These results show the effect of GNPs on the crystallization of PP, shifting the crystallization towards α crystals with expected higher mechanical performance.[29,30]

The dispersion behavior of GNP in different PP matrices

TEM and SEM analyses were performed to investigate the dispersion and interaction behavior of GNP sheets in Homo-PP and Copo-PP matrices. Figure 5 shows TEM images of Homo-PP/1 wt % GNP and Copo-PP/1 wt% GNP nanocomposites indicating proper interactions of GNPs in both polymer grades where particles are closely connected to the matrices without any sign of debonding at the interphase (additional TEM images are also provided in Fig. S3 at lower magnification). Figure 6 exhibits the freeze-fractured surface morphology of neat Homo-PP, neat Copo-PP and their nanocomposites with 1 wt% reinforcement. The fracture surface of neat specimens is smoother compared to their nanocomposite counterparts. However, it is worth noting that both neat Copo-PP and Copo-PP/1 wt% GNP exhibit some void in their structure which is not observed in Homo-PP based specimens due to the presence of ethylene groups. The higher void content of Copo-PP specimens can be another reason for their lower mechanical performance compared to Homo-PP counterparts (this will be discussed in the next section). On the other hand, uniform surface roughness in the fracture surface of Homo-PP/1 wt% GNP and Copo-PP/1 wt% GNP nanocomposites

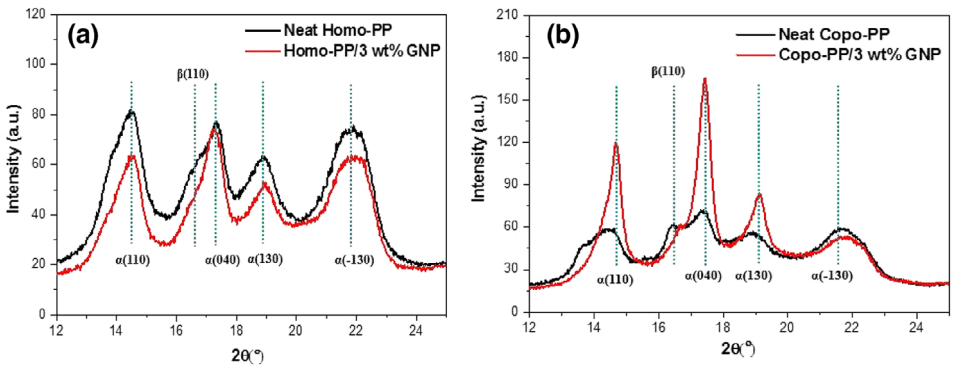

Figure 4. XRD patterns for (a) neat Homo-PP and Homo-PP/3 wt% GNP and (b) neat Copo-PP and Copo-PP/3 wt% GNP.

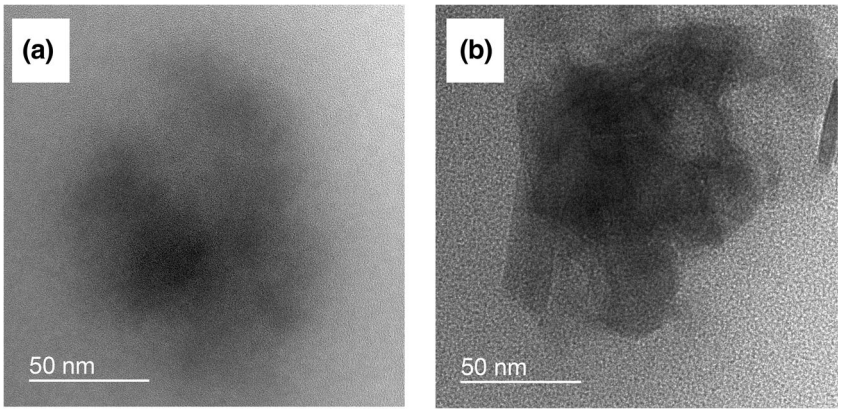

Figure 5. TEM images of (a) Homo-PP/1 wt% GNP and (b) Copo-PP/1 wt% GNP.

indicates homogeneous dispersion and proper exfoliation of GNPs in the matrix (additional SEM images are also provided in Fig. S4 at higher magnification).

Mechanical tests of GNP reinforced PP composites

The dimension of nanoscale GNP and the presence of various functional groups on their surface provide a great potential for this nanomaterial to be used as a reinforcing agent in various polymeric matrices to enhance the mechanical performance of polymeric structures. The nanoscale size of GNP is capable of alteration in the crystal structure of the polymeric matrix while their interface characteristics provide strong interfacial regions in contact with polymers leading to an effective load transfer from polymeric matrix to GNPs. Herein, GNPs were dispersed into both Copo-PP and Homo-PP polymers with a distinct chain structure and various crystallization capabilities under high shear rates by using a thermokinetic mixer; well-dispersed nanocomposites were formed. Then, dogbone shaped and rectangular composite specimens for tensile and bending tests, respectively, were prepared using an injection molding machine. The tensile and bending properties of each specimen type were studied to obtain an insight about the effect of GNPs on the mechanical performance of the developed structures.

Tensile tests

Figure 7 exhibits the tensile stress–strain curves of Homo-PP and Copo-PP nanocomposites loaded with various amounts of GNPs (ranging from 1 wt% to 5 wt%). The stress–strain curves of both

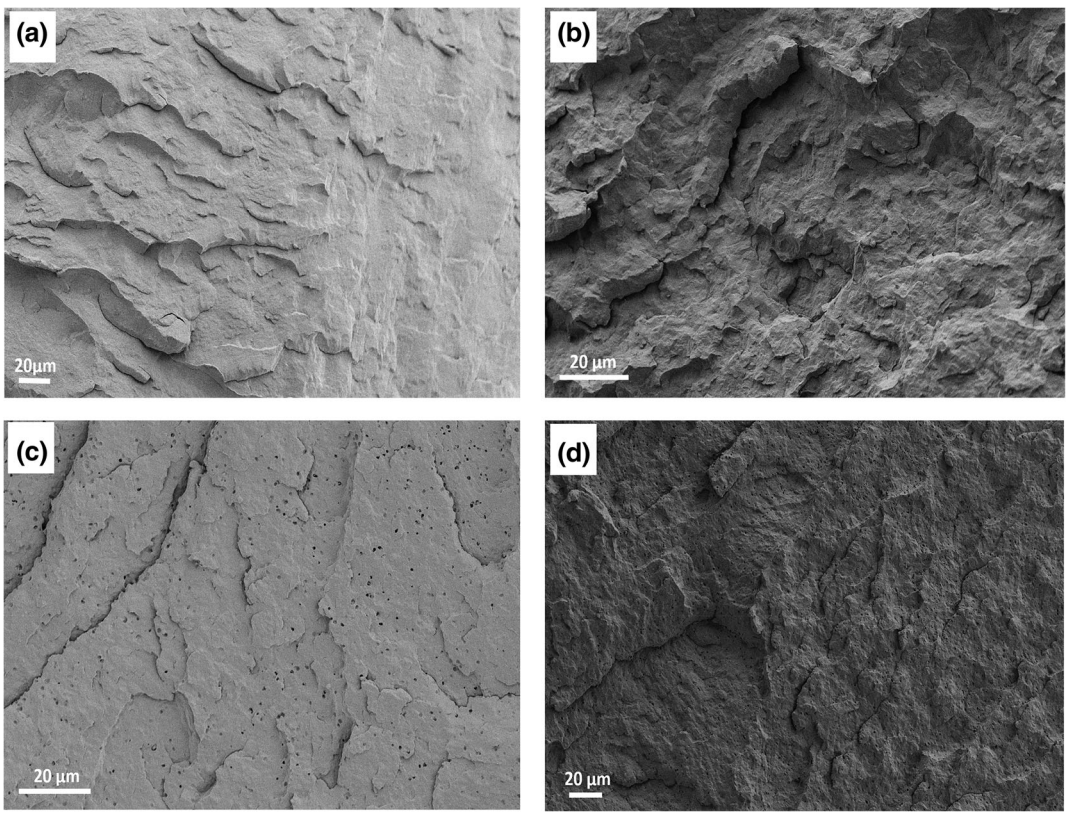

Figure 6. SEM images of freeze-fractured surfaces of (a) neat Homo-PP, (b) Homo-PP/1 wt% GNP, (c) neat Copo-PP and (d) Copo-PP/1 wt% GNP.

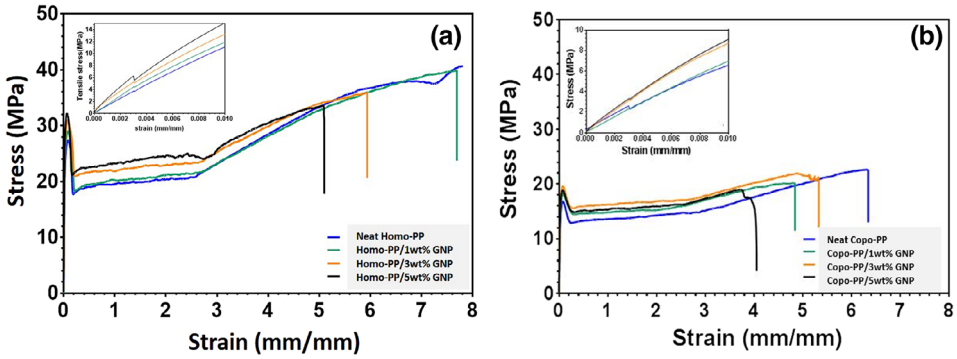

Figure 7. Tensile stress–strain curves of (a) Homo-PP/GNP and (b) Copo-PP/GNP nanocomposites.

composite types and their neat counterparts showed distinct regions of elastic elongation, yielding and plastic deformation or cold drawing. The inset graphs in both Fig. 7(a) and Fig. 7(b) represent the magnified initial stiff response or elastic elongation of specimens to applied loads at strain values under *ca* 0.01 mm mm^{-1}. The linear relation between stress and strain is clearly observed for both polymer grades and their nanocomposites in the aforementioned strain range. The values calculated for tensile modulus in the elastic response region indicate that the tensile modulus of neat Homo-PP is higher than that of neat Copo-PP because of different molecular structures and the higher crystallinity of Homo-PP polymer. Homo-PP nanocomposites showed an enhancement of about 18.5%, 27.4% and 50.8% in tensile modulus on the addition of 1, 3 and 5 wt% GNPs, respectively. On the other hand, the tensile modulus of Copo-PP was improved by 0.6%, 23.8% and 30.8% by the addition of 1, 3 and 5 wt% GNPs, respectively. The obtained improvements in the tensile modulus are also in agreement with other work reported in the literature.[9,34] Furthermore, yield strength, as the starting point of the plastic deformation of the specimens, is another crucial indication of the mechanical performance of polymeric structures and increased slightly on increasing the GNP content in both polymer grades. This confirms the proper dispersion of nano-reinforcement into both matrix types without any agglomerations which can create stress concentration sites.[35,36] A drop in stress value after the yield point indicates the strain softening phenomenon which is typical for thermoplastic polymers.[23] In the last part of the tensile test graphs, neat specimens and specimens reinforced by GNPs showed strain hardening due to an increase in chain orientation and strain-induced crystallization over 2.7 mm mm^{-1}. The strain hardening part of the graphs demonstrates that Homo-PP can have a higher amount of strain hardening compared to Copo-PP due to its linear molecular structure which enables it to have a higher ordering capability of chains and promotes crystallinity compared to Copo-PP polymers. The tensile strength as the maximum load seen by specimens during the tensile testing has a decreasing trend in both types of nanocomposites. Tensile strength is in close relation to strain at the failure of specimens and induced crystallization due to cold drawing and consequent strain hardening.[37] The existence of GNPs in the structure during the necking may disrupt chain orientation due to the size discrepancy between the size scale of GNPs and the orientation scale of chains which creates stress concentration sites and degrades the tensile strength and strain at failure of nanocomposite specimens. However, with increase in GNP content in both Homo-PP and Copo-PP, the strain at failure decreases owing to the difficulty of homogeneous dispersion and changes induced in the crystal structure and the creation of a nano-reinforcement network in the polymer matrix which prevents further cold crystallization in elongated sections.[38] It is worth noting that neat Homo-PP and its nanocomposites exhibit a higher modulus, yield strength, tensile strength and strain at failure compared to Copo-PP which is in agreement with their crystallinity differences discussed in detail in the section on crystallization. Nevertheless, in all cases, the mechanical properties of GNP reinforced Homo-PP and Copo-PP were higher than those of the neat polymers and this means that the reinforcement effect of GNP on these matrices except for elongation at break decreased continuously on increasing the GNP content. Table 2 summarizes the modulus and strength improvement percentages of the produced nanocomposites.

Table 2. Tensile modulus and tensile strength improvement percentages of GNP based PP nanocomposites

Specimen type	Modulus (MPa)	Improvement (%)	Tensile strength (MPa)	Yield strength (MPa)	Tensile strain at break (%)
Neat Homo-PP	1240 ± 38	—	40.6 ± 0.07	27.3	790 ± 3
Homo-PP/1 wt% GNP	1470 ± 70	18.5	39.8 ± 0.56	28.9	730 ± 33
Homo-PP/3 wt% GNP	1580 ± 75	27.4	36.4 ± 1.01	30.9	620 ± 22
Homo-PP/5 wt% GNP	1870 ± 39	50.8	32.4 ± 1.01	32	380 ± 169
Neat Copo-PP	780 ± 5	—	22.6 ± 0.10	16.3	640 ± 7
Copo-PP/1 wt% GNP	785 ± 10	0.6	20.5 ± 1.72	18	520 ± 74
Copo-PP/3 wt% GNP	966 ± 40	23.8	22 ± 0.5	19.8	545 ± 70
Copo-PP/5 wt% GNP	1020 ± 109	30.8	19.1 ± 0.83	18.5	410 ± 167

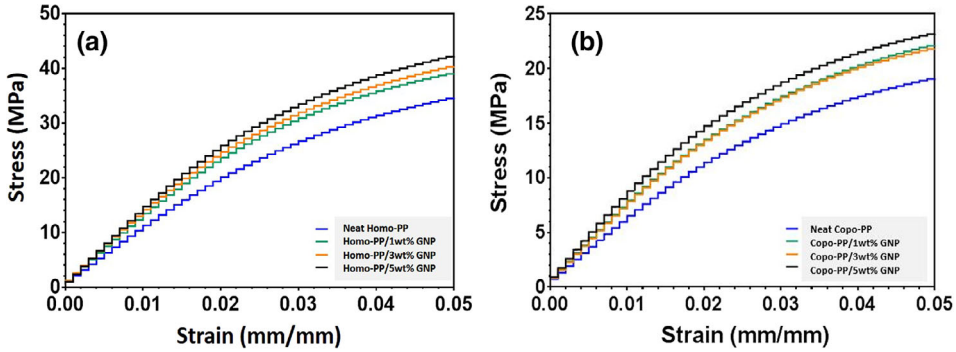

Figure 8. Flexural stress–strain curves of (a) Homo-PP/GNP and (b) Copo-PP/GNP nanocomposites.

Table 3. Chord modulus and flexural strength improvement percentages of GNP based PP nanocomposites

	Chord modulus (0.5%–1.0%) (MPa)	Improvement (%)	Flexural strength (MPa)	Improvement (%)
Neat Homo-PP	1010 ± 35	—	34.7 ± 0.95	—
Homo-PP/1 wt% GNP	1200 ± 24	18.8	39.1 ± 0.77	12.7
Homo-PP/3 wt% GNP	1270 ± 21	25.7	40.2 ± 0.48	15.9
Homo-PP/5 wt% GNP	1350 ± 33	33.6	42.5 ± 1.00	22.5
Neat Copo-PP	576 ± 5	—	19.2 ± 0.2	—
Copo-PP/1 wt% GNP	670 ± 34	16.3	21.7 ± 0.87	13.0
Copo-PP/3 wt% GNP	685 ± 3	18.9	21.8 ± 0.09	13.5
Copo-PP/5 wt% GNP	760 ± 17	31.9	23.2 ± 0.41	20.8

Flexural properties

The flexural properties are key parameters for the evaluation of the mechanical performance of composite structures and for understanding the interactions between matrix and reinforcement due to the complex stress profile induced in the specimens under test.[36,39] The representative flexural stress *versus* strain curves obtained from three-point bending tests for Homo- and Copo-PP based specimens are shown in Fig. 8. Two flexural property indices were obtained from these tests: the flexural modulus as a parameter for the tendency of the composite material to bend, and the flexural strength as a factor indicating the resistance of materials against fracture. The flexural test results

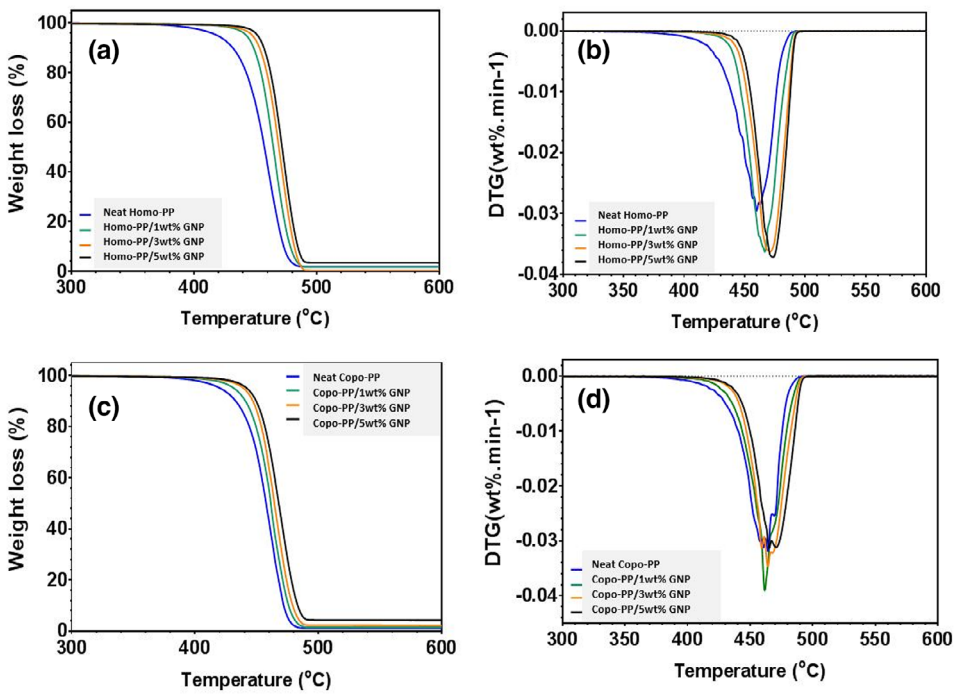

Figure 9. TGA analysis of Homo-PP, Copo-PP and their nanocomposites with GNPs.

showed that flexural modulus and flexural strength values of GNP reinforced composites were notably higher than those of neat Homo-PP and Copo-PP. In addition, it is seen that, on increasing the GNP content, the flexural modulus and flexural strength increased similarly in both cases (Table 3).

Thermogravimetric analysis (TGA)

The thermal stability of polymeric materials and their resistance to thermal degradation is a crucial property for many applications and can be improved by integration of nano-reinforcements. Figure 9 shows the TGA curves of neat Homo-PP and Copo-PP and their nanocomposites with GNPs. All samples showed a single step of degradation under an inert atmosphere. In both polymer grades, the onset temperature of decomposition was notably improved by GNPs. In the case of Homo-PP, the degradation onset temperature improved from 347 °C to higher temperatures on the incorporation of GNPs and reached 414 °C at 5 wt% GNPs. In a similar manner, for Copo-PP the onset temperature increased from 348 °C to about 400 °C on the addition of 5 wt% GNP. Therefore, the thermal stability of both PP types was remarkably amended in the presence of GNPs. This improvement in thermal stability of the nanocomposites is associated with the high thermal conductivity of GNPs which facilitates heat transfer in the nanocomposites and provides uniform heat distribution throughout the sample.[40]

CONCLUSION

In the present work, GNPs obtained from waste tires were dispersed homogeneously in Homo- and Copo-PP matrices with a thermokinetic mixer at high shear rates. The mechanical and thermal behaviors of PP based composites were examined simultaneously at different graphene loadings. DSC characterization results indicated that GNP acted as a nucleation agent and enhanced the crystallization of both Homo- and Copo-PP during the cooling cycles. Non-isothermal crystallization experiments showed that the crystallization temperature increased on increasing graphene content in both PP matrices and graphene nucleated crystallization in Homo-PP comparably more than in Copo-PP. Graphene promoted the growth of α crystals and eliminated the β phase in the structure and thus provided high mechanical performance. Tensile tests indicated that Homo-PP had a higher amount of strain hardening compared to Copo-PP due to its linear polymer chains and ordered structure. The flexural strength and modulus values of Homo-PP based nanocomposites were slighter higher than those of Copo-PP nanocomposites. As the graphene content increased in both polymer grades, the flexural properties of the fabricated specimens significantly increased. Both SEM and TEM images showed a proper dispersion of GNPs in the polymer matrix. Also, increasing the graphene content affected the thermal degradation behaviors of both Homo- and Copo-PP composites and the thermal stability of both types of composites was improved notably. In conclusion, graphene nanoplatelets have great potential to be used as a multi-functional additive in industrial applications since it can provide ease in the compounding process by eliminating binders and compatibilizers and other reagents used in compound formulation.

SUPPORTING INFORMATION

Supporting information may be found in the online version of this article.

REFERENCES

1 Iwamoto S, Yamamoto S, Lee SH, Endo T and Compos Part A, *Appl Sci Manuf* **59**:26–29 (2014).
2 Ashenai Ghasemi F, Ghasemi I, Menbari S, Ayaz M and Ashori A, *Polym Test* **53**:283–292 (2016).
3 Tripathi SN, Rao GSS, Mathur AB and Jasra R, *RSC Adv* **38**:23615–23632 (2017).
4 Jeon K, Chiari YL and Alamo RG, *Macromolecules* **41**:95–108 (2008).
5 Benavente R, Caveda S, Pérez E, Blazquez E, Peña B, van Grieken R *et al*., *Polym Eng Sci* **52**:2285–2295 (2012).
6 Milani MA, González D, Quijada R, Basso NRS, Cerrada ML, Azambuja DS *et al*., *Compos Sci Technol* **84**:1–7 (2013).
7 Kalaitzidou K, Fukushima H and Drzal LT, *Carbon* **45**:1446–1452 (2007).
8 Wang Z-J, Kwon D-J, Gu G-Y, Kim H-S, Kim D-S, Lee C-S *et al*., *Compos Sci Technol* **81**:69–75 (2013).
9 Vallés C, Abdelkader AM, Young RJ and Kinloch IA, *Faraday Discuss* **173**:379–390 (2014).
10 Li Y, Zhu J, Wei S, Ryu J, Sun L and Guo Z, *Macromol Chem Phys* **212**:1951–1959 (2011).
11 El Achaby M, Arrakhiz F-E, Vaudreuil S, el Kacem QA, Bousmina M and Fassi-Fehri O, *Polym Compos* **33**:733–744 (2012).
12 Ferreira CI, Dal Castel C, Oviedo MAS and Mauler RS, *Thermochim Acta* **553**:40–48 (2013).
13 Song P, Cao Z, Cai Y, Zhao L, Fang Z and Fu S, *Polymer* **52**:4001–4010 (2011).
14 Qiu F, Hao Y, Li X, Wang B and Wang M, *Compos Part B Eng* **71**:175–183 (2015).
15 William S, Hummers J and Offeman RE, *J Am Chem Soc* **80**:1339 (1958).
16 Ahmad SR, Xue C and Young RJ, *Mater Sci Eng B* **216**:2–9 (2017).
17 King JA, Klimek DR, Miskioglu I and Odegard GM, *J Compos Mater* **49**:659–668 (2015).
18 Kelnar I, Bal Ü, Zhigunov A, Kaprálková L, Fortelný I, Krejčíková S *et al*., *Compos Part B Eng* **144**:220–228 (2018).
19 Seretis GV, Manolakos DE and Provatidis CG, *Compos Part B Eng* **145**:81–89 (2018).
20 Park JS, Kim YS, Jung HJ, Park D, Yoo JY, Nam JH *et al*., *J Nanomater* **2019**:1–11 (2019).
21 Cakal Sarac E, Haghighi Poudeh L, Seyyed Monfared Zanjani J, Pehlivan ZS, Cebeci FÇ, Aydin I *et al*., *J Appl Polym Sci* **136**:1–11 (2019).
22 Saner Okan B, Turkish J, *Chem* **41**:381–390 (2017).
23 Seyyed Monfared Zanjani J, Saner Okan B and Menceloglu Y, *Mater Chem Phys* **176**:58–67 (2016).
24 Chen Y, Yin Q, Zhang X, Xue X and Jia H, *Thermochim Acta* **661**:124–136 (2018).
25 Beuguel Q, Boyer SAE, Settipani D, Monge G, Haudin J-M, Vergnes B *et al*., *Polym Cryst* **1**:1–10 (2018).
26 Broda J, Baczek M, Fabia J, Binias D and Fryczkowski R, *J Mater Sci* **55**:1436–1450 (2020).
27 Yang S, Li Y, Liang YY, Wang WJ, Luo Y, Xu JZ *et al*., *RSC Adv* **6**:23930–23941 (2016).
28 Ji X, Chen J-B, Zhong G-J, Li Z-M and Lei J, *J Thermoplast Compos Mater* **29**:1352–1368 (2016).
29 Nakamura K, Shimizu S, Umemoto S, Thierry A, Lotz B and Okui N, *Polym J* **40**:915–922 (2008).
30 Chen Y-H, Mao Y-M, Li Z-M and Hsiao BS, *Macromolecules* **43**:6760–6771 (2010).
31 Papageorgiou DG, Chrissafis K and Bikiaris DN, *Polym Rev* **55**:596–629 (2015).
32 Xu D and Wang Z, *Polymer* **49**:330–338 (2008).
33 Caballero MJ, Suarez I, Coto B, Van Grieken R and Monrabal B, *Macromol Symp* **257**:122–130 (2007).
34 Ashori A, Menbari S and Bahrami R, *J Ind Eng Chem* **38**:37–42 (2016).
35 Zanjani JSM, Saner Okan B, Menceloglu YZ and Yildiz M, *J Reinf Plast Compos* **34**:1273–1286 (2015).
36 Monfared Zanjani JS, Okan BS, Menceloglu YZ and Yildiz M, *RSC Adv* **6**:9495–9506 (2016).
37 Bikiaris D, *Materials* **3**:2884–2946 (2010).
38 Pegoretti A, Kolarik J, Peroni C and Migliaresi C, *Polymer* **45**:2751–2759 (2004).
39 Seyyed Monfared Zanjani J, Saner Okan B, Pappas P-N, Galiotis C, Menceloglu YZ and Yildiz M, *Compos Part A Appl Sci Manuf* **106**:1–10 (2018).
40 Cheng HKF, Chong MF, Liu E, Zhou K and Li L, *J Therm Anal Calorim* **117**:63–71 (2014).

